JOURNAL OF SPACECRAFT AND ROCKETS
Vol. 47, No. 4, July–August 2010

Engineering Notes

Effect of an Altitude-Dependent Background Atmosphere on Shuttle Plumes

Carolyn R. Kaplan* and Paul A. Bernhardt†
Naval Research Laboratory, Washington, D.C. 20375

DOI: 10.2514/1.47339

I. Introduction

THE shuttle ionospheric modification with pulsed localized exhaust (SIMPLEX) experiments conducted by the Naval Research Laboratory (NRL) were designed to 1) assess the effects of rocket exhaust interactions in the ionosphere and 2) mimic large ionospheric disturbances that occur naturally [1–5]. These experiments use space shuttle orbital maneuver subsystem (OMS) engines to inject exhaust over ground radar sites. The shuttle exhaust provides a high-speed neutral gas that streams through the ambient plasma of the ionosphere. The neutral exhaust molecules exchange charge with ambient O^+ ions in the ionosphere. This interaction between the plasma and neutrals results in the formation of ion-ring and beam velocity distributions of plasma particles in the ionosphere. During the SIMPLEX experiments, these distributions are studied with ground radars using incoherent scatter of radio waves from electrons in the ionosphere.

To date, six SIMPLEX burns [1–5] have been conducted over incoherent scatter radar sites at various locations, as shown in Table 1. In these experiments, the relative velocity between the ambient ions and injected neutrals is much faster than that which occurs naturally in any region of the ionosphere. Auroral electric fields can accelerate ions to velocities between 0.5 and 2.5 m/s [6]. The neutral injections from the space shuttle in orbit yield exhaust velocities of between 4.7 and 10.7 km/s relative to the background neutrals and ions. During the shuttle burn experiments, the high-speed neutrals chemically react with the stationary plasma. During auroral plasma convection, however, the high-speed ambient O^+ ions and electrons in the ionosphere (accelerated to a high velocity by auroral electric fields) chemically react with stationary neutral molecules or atoms [5,6]. Consequently, the primary difference between high-speed plasma convection and space shuttle OMS burns is the reference frame for the relative ion and neutral motion [5]; both phenomena result in the formation of ring-beam ion velocity distributions. The SIMPLEX experiments were designed to reproduce the naturally occurring ion-ring distributions, which can create ionospheric instabilities leading to regions of plasma turbulence. In addition, the experiments also provide a unique way to examine gas-phase physical and chemical phenomena in the hypersonic and hyperthermal energy regime, which is relatively unstudied and difficult to reproduce in a laboratory [7].

Received 24 September 2009; revision received 26 February 2010; accepted for publication 1 April 2010.

*Research Chemical Engineer, Laboratory for Computational Physics and Fluid Dynamics, Code 6410. Associate Fellow AIAA.

†Research Physicist, Plasma Physics Division, Code 6754.

The first step to modeling the ionospheric interactions of space shuttle exhaust is to describe the neutral flow from the exit plane of the shuttle OMS engines into the expanse of the upper atmosphere. In this paper, we use the direct simulation Monte–Carlo (DSMC) method [8] to simulate the shuttle burn and to study the interaction between the shuttle exhaust and the neutral species of the background atmosphere. In the following sections, we present simulation results showing the time evolution of the shuttle plume and background, and we discuss the effect of the altitude-dependence of the background atmosphere.

II. Numerical Model

The simulations were carried out with a two-dimensional, time-dependent DSMC code, that uses variable hard sphere (VHS) particles with the modified no-time-counter scheme [9] to select collision pairs, and includes translational-rotational energy exchange based on the Larsen–Borgnakke model [10]. A schematic of the computational domain is shown in Fig. 1a. Since the goal of this work is to study the time evolution of the shuttle exhaust and its interaction with the background atmosphere, the computational domain spans an area of 400 km in width by 200 km in height. These calculations do not include the shuttle geometry, because the size of the shuttle is negligible in relation to the computational domain, and we are not investigating spacecraft contamination.

The simulations presented here correspond to *ram burns*, in which the OMS engines are oriented in the same direction as the shuttle orbit. The SIMPLEX experiments associated with STS-93, −108 and −110 were ram burns. The other experiments that used out-of-plane burns will be described in future papers. The shuttle is modeled as a moving source, traveling at 7.72 km/s at an altitude of 300 km, while the velocity of the exhaust, relative to the shuttle, is 3.07 km/s. The shuttle exhaust produces an efflux of 5×10^{26} molecules, at 120 K, over a time period of 10 s, and consists of the following species and mole fractions: N_2: 0.32, H_2O: 0.28, H_2: 0.25, CO_2: 0.15. This corresponds to the simultaneous firing of both OMS engines on the space shuttle.

The background atmosphere includes the species O, O_2 and N_2 whose concentrations are altitude-dependent, and are calculated with the NRL mass spectrometer incoherent scatter (MSIS) radar model [11]. MSIS describes the concentration and temperature of the neutral atmosphere from the surface to the lower exosphere, as a function of date, time, altitude, latitude, longitude, solar flux and magnetic index. During the initialization subroutine, the DSMC code calls MSIS to calculate the macroscopic concentration and temperature in each computational cell, and then generates particles sampled from a Maxwellian distribution. Figure 1b shows the number density and temperature of the background neutral atmosphere species, used as the initial condition in the calculation.

The DSMC code uses a stretched Cartesian mesh, in which cell dimensions are less than the local mean free path. Flowfield cells are 150 × 150 m at the lower boundary and left boundary where the number density of the background atmosphere (at $y = 200$ km) and shuttle exhaust (at $x = 0$ km) are greatest, respectively. At the upper ($y = 400$ km) and right ($x = 400$ km) boundaries, flowfield cell dimensions are stretched to 1500 × 1500 m. Boundary conditions at all four boundaries are specified as a subsonic fixed pressure condition [12], where the pressure is calculated based on the local MSIS atmosphere conditions. At $x = 0$ and $x = 400$ km, the fixed pressure, P, in each boundary cell is altitude-dependent, while at $y = 200$ km, $P = 1.2 \times 10^{-4}$ N/m^2, and at $y = 400$ km, $P = 3.4 \times 10^{-6}$ N/m^2. The shuttle exhaust is modeled as a jet with a velocity of 10.79 km/s, and a standard DSMC acceptance-rejection method for sampling from a prescribed distribution [8] is used to generate

Table 1 SIMPLEX experiments and associated shuttle flights

Experiment number	Observatory	Date	Shuttle flight
1	Jicamarca Radio, Peru	Oct. 1997	STS-86
2	Arecibo, Puerto Rico	July 1999	STS-93
3	Millstone Hill, Massachusetts	Dec. 2001	STS-108
4	Millstone Hill, Massachusetts	April 2002	STS-110
5	Millstone Hill, Massachusetts	March 2009	STS-119
6	Millstone Hill, Massachusetts	Sept. 2009	STS-128

velocity components for each jet molecule. The simulations presented below contain 54 million particles, with 800×400 flowfield cells, and four subcells per flowfield cell for collision sampling. Time steps are 0.05 s, which is well below the mean collision time of 0.2 s in the highest-density regions. Ensemble-average sampling is used to obtain the time-dependent solution.

III. Results

Figure 2 shows the number density of the water vapor and atomic oxygen at 10, 20, and 30 s of physical time after motor ignition. Water is one of the main constituents of the shuttle exhaust; therefore, the images on the left represent the evolution of the plume from the OMS engine. The first H_2O image corresponds to the plume at the end of the 10 s burn; the continuous release of exhaust during those 10 s is evidenced by the solid red region. After 10 s, the output flow ceases, and the shape of the plume at 20 and 30 s is characterized by the plume's interaction with the surrounding atmosphere. The atomic oxygen images on the right represent the response of the altitude-dependent background atmosphere to the shuttle exhaust. As shown, the exhaust plume displaces the surrounding atmosphere, and, by 30 s, a shell of dense atomic oxygen has formed at the lower altitude. The shape of the exhaust plume and the displacement of the background atmosphere is vertically asymmetric, due to the fact that the atmosphere number density decreases with altitude.

The effect of the structure of the background atmosphere is illustrated in Fig. 3, which shows various quantities at 25 s after burn start. Images on the left correspond to the altitude-dependent surrounding atmosphere, while those on the right correspond to a uniform background atmosphere. For the uniform case, the atmospheric concentration and temperature are calculated from MSIS at the burn altitude (300 km). The differences between the two sets of images indicate that the altitude-dependent background distorts the shape of the plume, as the greater atmospheric density and pressure at the lower altitudes creates more drag on the lower part of the plume. The velocity vectors indicate that, for the altitude-dependent case, the upper portion of the plume has a greater vertical velocity, which also contributes to the skewed plume shape. As shown in the velocity images, the structure of the background atmosphere also affects the velocity profile in the low-pressure wake-flow region. The significant differences in the shapes of plume species H_2 and CO_2 is due to their differences in mass diffusivity. The lighter H_2 diffuses more quickly with the background atmosphere, compared with the heavier CO_2.

As discussed earlier, the calculations shown in Figs. 2 and 3 result from a simulation using 54 million molecules. To show that the calculations were adequately resolved, the same simulation was also conducted using 27 million molecules. Figure 4 shows line contours of H_2O vapor number density, at 10 s after burn start, for the two calculations, superimposed on top of one another. The only discernible difference is that the calculation with fewer molecules contains more statistical noise. As shown by the results at 10-s (end of the burn) in Fig. 4, and by the time sequence shown in Fig. 2, it can be seen that the degree of asymmetry increases with time. This is because at the longer times, the plume has had more interaction with the background atmosphere, and since the atmosphere is less dense at the higher altitudes, the plume becomes more asymmetric as time progresses.

The results presented in Figs. 2–4 are for a ram burn, in which the OMS engines are oriented in the same direction as the shuttle orbit. Results of additional simulations for a perpendicular burn (not shown), in which the OMS engines are oriented 90 deg from the shuttle orbit direction, show that including an altitude-dependent background atmosphere results in a slightly taller plume, but that the effects of the nonuniform atmosphere are less significant compared with the ram burn scenario.

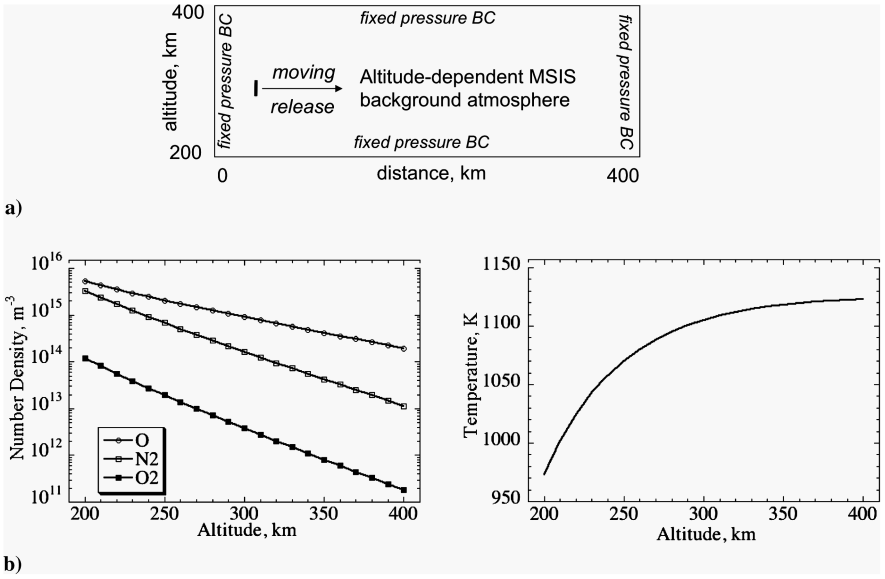

Fig. 1 a) Schematic of the computational domain and b) number density and temperature of the background atmosphere, as a function of altitude, at initialization.

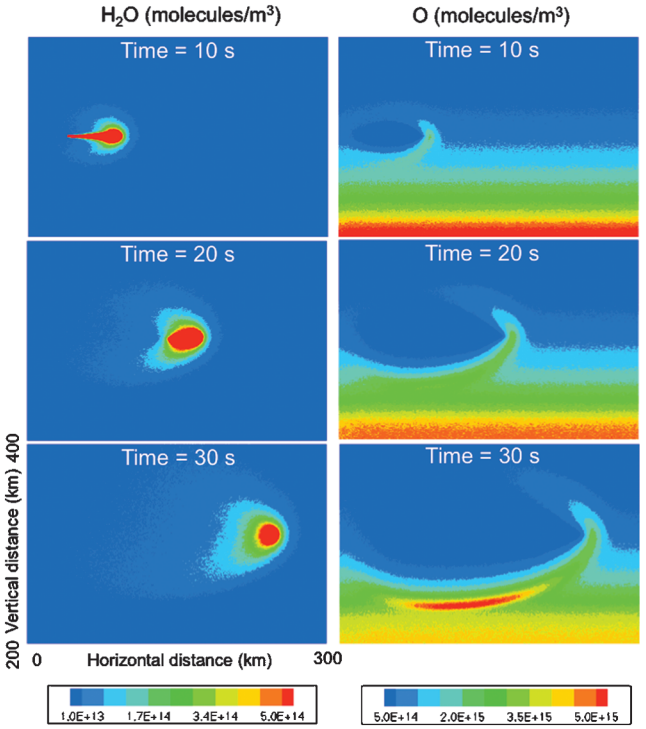

Fig. 2 Water vapor and atomic oxygen number density at 10, 20, and 30 s after the start of the burn.

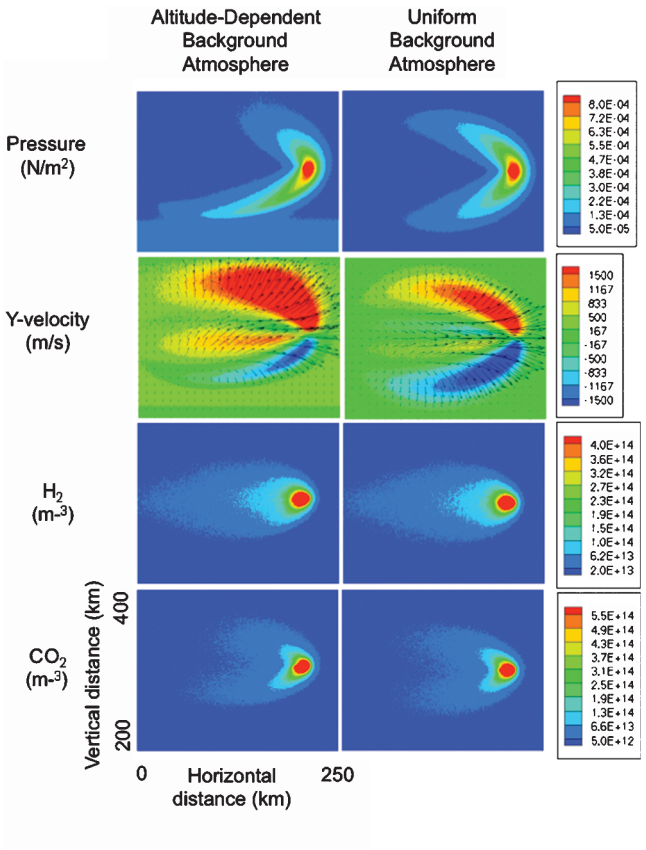

Fig. 3 Indicated quantities at 25 s after burn start. Velocity vectors are superimposed on the *y*-velocity image.

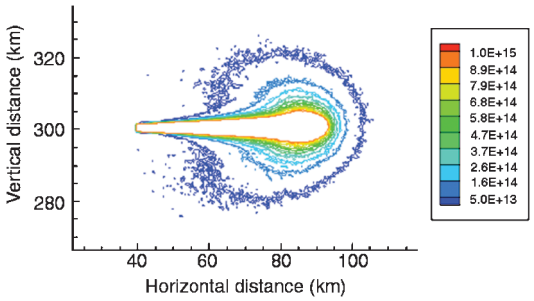

Fig. 4 Water vapor number density at 10 s after burn start for the altitude-dependent background atmosphere scenario. Results at two resolutions (54 million molecules vs 27 million molecules) are superimposed on top of each other.

IV. Conclusions

Time-dependent DSMC calculations are presented to simulate the shuttle burns associated with the NRL SIMPLEX experiments, and to study the interactions between the shuttle exhaust and the neutral species of the background atmosphere. The calculations show that when the altitude-dependence of the background atmosphere is included in the simulation initial conditions, the shape of the shuttle exhaust plume is skewed. This is because the greater atmospheric density and pressure at the lower altitudes creates more drag on the lower part of the plume.

Recent experiments by Dimpfl et al. [7] have measured the size and shape of the radiance from midultraviolet Cameron band emission from carbon monoxide in the plumes of space shuttle OMS engines. Images of radiance from their experiments showed a skewed-shape plume, which differed from the shape obtained from their DSMC calculations using a uniform background atmosphere. To match the plume size and shape between their experiments and simulations, they developed an extended variable hard sphere and variable soft sphere model, which invokes chemical dynamics involving a first step with highly nonisotropic forward scattering, to extend the validity of scattering treatment to hyperthermal collision energies [13]. In the simulations presented here, we use the traditional VHS isotropic scattering treatment [8,9], and a skewed plume shape is obtained due to the effects of the altitude-dependent background atmosphere.

The results of Dimpfl et al. [7,13] were for a 37 s burn, and their UV bandpass images were obtained over the duration of that burn, so that it could be considered to represent a steady plume. Likewise, their DSMC calculations were of a steady, axisymmetric plume. In contrast, the calculations presented here are for a 10-s burn, and our DSMC calculations focus on the time-dependent interaction between the plume and the altitude-dependent background atmosphere. Although the two studies both investigate shuttle OMS engine burns and an asymmetric plume that results from its interaction with the ionosphere, they each focus on different aspects of the process: the work of Dimpfl et al. focuses on the chemical dynamics of a steady plume, while our work focuses on the fluid dynamics of a time-dependent plume. Further study is needed to sort out the contributions of each of the mechanisms (chemical vs fluid dynamics) to the observed plume asymmetry.

Validation of our large-scale DSMC computations will be attempted using optical emissions that result from the recombination of the charge-exchange ions and electrons. That is, after the charge-exchange reaction between the neutral exhaust and the ambient ions ($H_2O + O^+ \Rightarrow H_2O^+ + O$), recombination reactions occur between the charge-exchange ions and electrons ($H_2O^+ + e^- \Rightarrow OH + H$), which produce optical emissions. The generation of artificial airglow clouds from exhaust releases in the ionosphere was first proposed by Bernhardt in 1976 [14] and subsequently observed in many experiments [15]. The optical clouds travel along a path downstream from the exhaust injection, similar to that illustrated on the left side of Fig. 2. The position of the optical emissions are affected by both the position of the neutral exhaust cloud and the density of ionospheric O^+ ions in the neutral flowfield. Quantitative

comparison of the observed enhancements in recombination airglow will require the additional step of following the charge-exchange ion motion along magnetic field lines until ion-electron recombination occurs. The magnitudes of the offsets for the optical emissions are consistent with the computations in this paper. Near-term future computational plans are to add the ion-molecule charge-exchange and ion-electron recombination reactions to further investigate the ion-ring and beam velocity distributions observed in the SIMPLEX experiments.

Acknowledgment

The authors gratefully acknowledge financial support from the Office of Naval Research through Naval Research Laboratory 6.2 funds.

References

[1] Bernhardt, P. A., Ganguli, G., Kelley, M. C., and Swartz, W. E., "Enhanced Radar Backscatter from Space Shuttle Exhaust in the Ionosphere," *Journal of Geophysical Research*, Vol. 100, No. A12, 1995, pp. 23811–23818. doi:10.1029/95JA02836

[2] Bernhardt, P. A., Huba, J. D., Swartz, W. E., and Kelley, M. C., "Incoherent Scatter from Space Shuttle and Rocket Engine Plumes in the Ionosphere," *Journal of Geophysical Research*, Vol. 103, No. A2, 1998, pp. 2239–2251. doi:10.1029/97JA02866

[3] Bernhardt, P. A., Huba, J. D., Kudeki, E., Woodman, R. F., Condori, L., and Vullaneuva, F., "Lifetime of a Depression in the Plasma Density over Jicamarca Produced by Space Shuttle Exhaust in the Ionosphere," *Radio Science*, Vol. 36, No. 5, 2001, pp. 1209–1220. doi:10.1029/2000RS002434

[4] Bernhardt, P. A., and Sulzer, M. P., "Incoherent Scatter Measurements of Ring-Ion Beam Distributions Produced by Space Shuttle Exhaust Injections into the Ionosphere," *Journal of Geophysical Research*, Vol. 109, 2004, p. A02303. doi:10.1029/2002JA009693

[5] Bernhardt, P. A., Erickson, P. J., Lind, F. D., Foster, J. C., and Reinisch, B. W., "Artificial Disturbances of the Ionosphere over the Millstone Hill Incoherent Scatter Radar from Dedicated Burns of the Space Shuttle Orbital Maneuver Subsystem Engines," *Journal of Geophysical Research*, Vol. 110, 2005, p. A05311. doi:10.1029/2004JA010795

[6] Gaimard, P., Lathuillere, C., and Hubert, D., "Non-Maxwellian Studies in the Auroral F Region: A New Analysis of Incoherent Scatter Spectra," *Journal of Atmospheric and Terrestrial Physics*, Vol. 58, Nos. 1–4, 1996, pp. 415–433. doi:10.1016/0021-9169(95)00046-1

[7] Dimpfl, W. L., Light, G. C., and Bernstein, L. S., "Molecular Dynamics from Remote Observation of CO(a) from Space Shuttle Plumes," *Journal of Spacecraft and Rockets*, Vol. 42, No. 2, 2005, pp. 352–362. doi:10.2514/1.7601

[8] Bird, G. A., *Molecular Gas Dynamics and the Direct Simulation of Gas Flows*, Clarendon Press, Oxford, 1994.

[9] Bird, G. A., "Sophisticated DSMC," http://www.gab.com.au/Resources/DSMC07notes.pdf [retrieved 24 Sept. 2009].

[10] Borgnakke, C., and Larsen, P. S., "Statistical Collision Model for Monte–Carlo Simulation of Polyatomic Gas Mixture," *Journal of Computational Physics*, Vol. 18, No. 4, 1975, pp. 405–420. doi:10.1016/0021-9991(75)90094-7

[11] Picone, J. M., Hedin, A. E., Drob, D. P., and Aikin, A. C., "NRLMSISE-00 Empirical Model of the Atmosphere: Statistical Comparisons and Scientific Issues," *Journal of Geophysical Research*, Vol. 107(A12), 2002, p. 1468. doi:10.1029/2002JA009430

[12] Nance, R. P., Hash, D. B., and Hassan, H. A., "Role of Boundary Conditions in Monte–Carlo Simulation of Microelectromechanical Systems," *Journal of Thermophysics and Heat Transfer*, Vol. 12, No. 3, 1998, pp. 447–449. doi:10.2514/2.6358

[13] Dimpfl, W. L., Wysong, I. J., Gimelshein, S. F., Braunstein, M., and Bernstein, L. S., "Application of the Born–Mayer Potential with a Hard-Sphere Scattering Kernel to Rarefied Hyperthermal Gas Flow Modeling," *Rarefied Gas Dynamics*, edited by T. Abe, Vol. 1084, AIAA, Reston, VA, 2008, pp. 323–328. doi:10.1063/1.3076494

[14] Bernhardt, P. A., "The Response of the Ionosphere to the Injection of Chemically Reactive Vapors," Stanford Univ. Radioscience Lab., TR 17, Stanford, CA, May 1976.

[15] Mendillo, M., "Ionospheric Holes: A Review of Theory and Recent Experiments," *Advances in Space Research*, Vol. 8, No. 1, 1988, pp. 51–62. doi:10.1016/0273-1177(88)90342-0

I. Boyd
Associate Editor